


 Cite this: *RSC Adv.*, 2023, **13**, 4590

## Modeling of Sandia Flame D with the non-adiabatic chemistry tabulation approach: the effects of different laminar flames on NO<sub>x</sub> prediction†

 Chuanfeng Yue, <sup>ab</sup> Jingbo Wang <sup>\*ab</sup> and Xiangyuan Li <sup>ab</sup>

The effects of different one-dimensional laminar flames on the prediction of nitrogen oxide (NO<sub>x</sub>) emission in Sandia Flame D are numerically investigated using a flamelet method in the present work. In addition to the basic control variables of the mixture fraction and the reaction progress variable for chemistry tabulation in this combustion model, two additional variables of mixture fraction variance and enthalpy loss are added to the control variable space to improve prediction accuracy of the NO<sub>x</sub> pollutant. The former variable of mixture fraction variance is used for the presumed probability density function integration, and the latter takes into account the non-adiabatic effect. Two flamelet libraries are generated based on the one-dimensional unstretched premixed flame and the one-dimensional counterflow diffusion flame, respectively. An additional transport equation for the mass fraction of nitrogen oxide (NO) is solved for improving prediction accuracy. The unsteady Reynolds-averaged Navier–Stokes (URANS) simulation results are compared and analyzed with experimental data. The simulation results show dependence on the type of laminar flame. In the four-dimensional control variable space, the results with steady unstretched premixed flame indicate great agreement on the predictions of temperature and NO field. The computational method proposed in the present work sheds light on the high-precision combustion numerical simulation of NO<sub>x</sub> emission.

 Received 27th September 2022  
 Accepted 21st January 2023

 DOI: 10.1039/d2ra06075b  
[rsc.li/rsc-advances](http://rsc.li/rsc-advances)

### 1. Introduction

With the increasing attention of pollution issues, the emission reduction of pollutants such as nitrogen oxides (NO<sub>x</sub>) has become one of the important indicators in the development of gas turbines and internal combustion engines. While computational fluid dynamics (CFD) is utilized as a powerful design approach in the motivation to design high performance and clean burners,<sup>1</sup> one-step or global reaction mechanisms are widely used in engineering simulation applications due to limited computational resources. However, NO<sub>x</sub> emission predictions given in these conditions are inaccurate due to the oversimplified chemical mechanism leading to incomplete related reactions.<sup>2–8</sup> High-precision chemical mechanisms frequently containing thousands of species for hydrocarbons<sup>3</sup> bring unacceptable computational cost. Therefore, the application of the high-precision chemical kinetic models in combustion simulations has become an important research topic.<sup>4–13</sup>

Recent advances in combustion modeling to reduce the computational cost of application of detailed chemical kinetics are the development of flamelet-like models,<sup>14–16</sup> such as flame prolongation of intrinsic low-dimensional manifolds (FPI),<sup>17</sup> steady laminar flamelet model (SLFM),<sup>18</sup> flamelet/progress variable (FPV)<sup>19</sup> and flamelet generated manifold (FGM).<sup>20</sup> These combustion models share the same basic assumption that the high-dimensional real flame consists of a series of low-dimensional flamelets. It means that the species distribution in turbulent combustion (high-dimensional) can be estimated by the low-dimensional manifolds (LDM). The FGM model developed by Oijen *et al.*<sup>21</sup> have two basic control variables of mixture fraction ( $\mathcal{Z}$ ) and progress variable ( $\mathcal{Y}$ ). The FGM library is built by mapping thermophysical parameters such as species mass fractions in different states to the control variable space. However, the errors are inevitable for the operation of directly look-up NO<sub>x</sub> mass fraction in the library due to the different characteristic time scales of  $\mathcal{Y}$  and NO<sub>x</sub>.<sup>6,22,23</sup>

Many works on NO<sub>x</sub> modeling with flamelet-like approaches have been reported in literature. Ihme *et al.*<sup>24</sup> performed LES/FPV simulations of turbulent non-premixed flames. They found that NO emission (the main component of NO<sub>x</sub> emission) prediction could be improved by adding additional NO transport equation and modeling the consumption component in the NO source term separately. Considering the larger time scale of NO, Godel *et al.*<sup>22</sup> proposed a novel  $\mathcal{Y}$  definition by

<sup>a</sup>College of Chemical Engineering, Sichuan University, Chengdu, 610065, P. R. China.  
 E-mail: [wangjbingbo@scu.edu.cn](mailto:wangjbingbo@scu.edu.cn)

<sup>b</sup>Engineering Research Center of Combustion and Cooling for Aerospace Power, Ministry of Education, Sichuan University, Chengdu, 610065, P. R. China

† Electronic supplementary information (ESI) available. See DOI: <https://doi.org/10.1039/d2ra06075b>



additional including  $\text{NO}_x$  species that could captures better NO evolution. Similarly, Akargun *et al.*<sup>25</sup> built the extended FGM table by optimizing the definition of PV for key parameters such as soot and  $\text{NO}_x$  for non-premixed combustion. Various tests of different ways to modeling  $\text{NO}_x$  formation with FGM method are performed by Tang *et al.*<sup>26</sup> which indicated that the prediction of NO can be improved effectively by considering radiation. Due to some key parameters of the steady diffusion flamelet will affect the accuracy of simulation results, such as temperature and NO concentration, Yao *et al.*<sup>27</sup> proposed a procedure to optimize flamelet parameters by using the surrogate assisted evolutionary algorithm. The LES/FGM simulation of  $\text{CH}_4/\text{NH}_3/\text{air}$  swirl flames<sup>28</sup> demonstrated that the  $\text{NH}_3$  concentration, residence time and temperature are important factors to effect the concentration distribution of NO. Recently, Zhang *et al.*<sup>29</sup> investigated the effect of transport properties on near-wall temperature by using uniform and non-uniform Lewis number (Le) in LES/FGM simulation.

According to the literature, the flamelet library can be constructed with one-dimensional laminar premixed flame or with one-dimensional laminar counterflow diffusion flame. The former is used to study flame propagation problems, and the latter is applicable to diffusion flames, auto-ignition and extinction (scalar dissipation rate plays a very important role). Generally, the first step is to determine which one-dimensional laminar flame is more similar to the flame structure in the CFD simulation when using a flamelet-like model for chemistry tabulation. However, there is no clear answer to this question, especially for the prediction of  $\text{NO}_x$  emission. In present work, the effects of two one-dimensional laminar flames, unstretched premixed (UP) flame and counterflow diffusion (CD) flame, on the prediction of  $\text{NO}_x$  emission in Sandia Flame D are investigated by unsteady Reynolds-averaged Navier-Stokes (URANS) method with a customized solver developed on the platform of OpenFOAM.<sup>30,31</sup> Since the flamelet library generated with the basic variables of  $Z$  and  $Y$  cannot predict  $\text{NO}_x$  emission well, present study takes into account the turbulence-chemical-radiation-interaction (TCRI) by adding additional control variables of mixture fraction variance and enthalpy loss. The rest of present work consists of three parts. Section 2 briefly introduces the mathematical methods of turbulent combustion, case configuration and numerical setup. The effect of the two flamelet libraries on flame structure and  $\text{NO}_x$  emission are discussed in Section 3. The main findings are summarized in Section 4.

## 2. Methodology

### 2.1. Governing equations

The solution strategy of using the URANS model and the chemistry tabulation approach to simulate the Sandia Flame D in current study is summarized as following steps:

(i) With the definition of the variables of  $Z$ ,  $Y$  and enthalpy loss, a series of two kinds of laminar flames, UP flame and CD flame, are solved and transformed to obtain the corresponding laminar flamelets, respectively.

(ii) The variance of the mixture fraction is defined and add to the control variables space for the  $\beta$  probability density function ( $\beta$ -PDF) integration. And the turbulent flamelets library is obtained by presumed PDF integration.

(iii) Solving the governing equations including control variables in CFD solver and thermo-chemistry variables are updated by the flamelet library.

The governing equations for mass, momentum, control variables are expressed as follows:

$$\frac{\partial \bar{\rho}}{\partial t} + \frac{\partial(\bar{\rho}\tilde{u}_i)}{\partial x_i} = 0 \quad (1)$$

$$\frac{\partial}{\partial t}(\bar{\rho}\tilde{u}_i) + \frac{\partial \bar{\rho}\rho\tilde{u}_i\tilde{u}_j}{\partial x_j} = \frac{\partial \bar{\sigma}_{ij}}{\partial x_j} + \frac{\partial}{\partial x_j} \left( -\bar{\rho}\tilde{u}'_i\tilde{u}'_j \right) \quad (2)$$

$$\frac{\partial(\bar{\rho}\tilde{h})}{\partial t} + \frac{\partial(\bar{\rho}\tilde{u}_i\tilde{h})}{\partial x_i} = \frac{\partial}{\partial x_i} \left( D_{\delta h} \frac{\partial \tilde{h}}{\partial x_i} \right) - \bar{S}_h \quad (3)$$

$$\frac{\partial(\bar{\rho}\tilde{Z})}{\partial t} + \frac{\partial(\bar{\rho}\tilde{u}_i\tilde{Z})}{\partial x_i} = \frac{\partial}{\partial x_i} \left( D_Z \frac{\partial \tilde{Z}}{\partial x_i} \right) \quad (4)$$

$$\begin{aligned} \frac{\partial}{\partial t}(\bar{\rho}\tilde{Z}'') + \frac{\partial \bar{\rho}\tilde{u}_i\tilde{Z}''^2}{\partial x_i} &= \frac{\partial}{\partial x_i} \left( D_{Z''^2} \frac{\partial \tilde{Z}''^2}{\partial x_i} \right) \\ &+ C_1 D_{Z''} \left| \frac{\partial \tilde{Z}''}{\partial x_i} \right|^2 - C_2 \bar{\rho} \widetilde{S}_X \end{aligned} \quad (5)$$

$$\frac{\partial}{\partial t}(\bar{\rho}\tilde{Y}) + \frac{\partial \bar{\rho}\tilde{u}_i\tilde{Y}}{\partial x_i} = \frac{\partial}{\partial x_i} \left( D_Y \frac{\partial \tilde{Y}}{\partial x_i} \right) + \bar{\omega} \quad (6)$$

where  $\rho$ ,  $u_i$ ,  $\delta_h$ ,  $Z$ ,  $Z''^2$ ,  $Y$  are density, velocity, enthalpy loss, mixture fraction, variance of mixture fraction and progress variable, respectively. The superscript  $-$ ,  $\sim$  means unweighted average and density weighted average. Tensor  $\sigma_{ij}$  defined as

$$\sigma_{ij} = 2\mu(S_{ij} - S_{kk}\delta_{ij}/3) - p\delta_{ij} \quad (7)$$

where  $S_{ij}$  is strain rates,

$$S_{ij} = \frac{1}{2} \left( \frac{\partial u_i}{\partial x_j} + \frac{\partial u_j}{\partial x_i} \right) \quad (8)$$

According to Boussinesq's hypothesis, Reynolds stress  $R_{ij}$  is given by

$$R_{ij} = -\bar{\rho}\tilde{u}'_i\tilde{u}'_j = \frac{1}{3}R_{kk}\delta_{ij} + 2\mu_t \left( \widetilde{S}_{ij} - \frac{1}{3}\widetilde{S}_{kk}\delta_{ij} \right) \quad (9)$$

$D_{\delta h}$  is the effective thermal conductivity of the mixture,  $D_{\delta h} = \alpha + \mu_t/\text{Pr}_t$ .  $\alpha$  is laminar diffusion coefficient,  $\text{Pr}_t$  is turbulent Prandtl number.  $D_z$ ,  $D_{Z''^2}$  and  $D_Y$  are effective dynamic viscosity of mixture fraction, variance of mixture fraction, and process variables, respectively. According to the unity Lewis number assumption, they can be expressed as



$D_Z = D_{Z''^2} = D_Y = \mu/Sc + \mu_t/Sc_t$  with  $r = 1.0$ ,  $Sc_t = Pr_t = 0.7$ .  $\mu$  and  $\mu_t$  are molecular and turbulent viscosity,  $\mu = \lambda/C_p$ ,  $\mu_t = \rho C_\mu k^2/\varepsilon$ .  $k$  is the turbulent kinetic energy,  $\varepsilon$  is the turbulent dissipation rate for the standard  $k-\varepsilon$  turbulence model.<sup>32</sup> Compared with the predictions of the  $k-\omega$ -SST model that is commonly used in engineering simulation, the standard  $k-\varepsilon$  model gives more accurate temperature peaks and corresponding reasonable NO peaks on the central axis. The results are shown in Fig. S1 of the ESI.† So turbulent scalar dissipation rate of mixture fraction  $\tilde{S}_x$  is defined as  $\tilde{S}_x = \varepsilon/k\tilde{Z}''^2$ . For constant numbers in eqn (5),  $C_1 = C_2 = 2.0$ . The radiation effect is considered in present work and the radiation model of optical thin model (OTM) is adopted.<sup>33,34</sup>  $S_h$  is source term of radiation.

$$S_h(T, \text{species}) = 4\sigma(T^4 - T_b^4) \sum (p_i a_{p,i}) \quad (10)$$

where Stefan-Boltzmann constant  $\sigma$  equals to  $5.669 \times 10^{-8} \text{ W} (\text{m}^2 \text{ K}^4)^{-1}$ .  $p_i$  is the partial pressure of species  $i$  in atmosphere.  $a_{p,i}$  is the Planck mean absorption coefficient of species.  $T$  is the local flame temperature and  $T_b$  is the background temperature. Species considered for radiation include  $\text{CO}_2$ ,  $\text{CO}$ ,  $\text{H}_2\text{O}$  and  $\text{CH}_4$ . Finally, governing equations are closed by the equation of state of ideal gas.

## 2.2. Flamelet library generation and TCRI

The two one-dimensional laminar flames are calculated using FlameMaster.<sup>35</sup> A series of mixture fraction  $Z$  are used to change the equivalent ratio of inlet boundary for building UP library. Mixture fraction  $Z$  is defined by Bilger's formulation.<sup>36</sup>

$$Z = \frac{0.5(Y_H - Y_H^2)/W_H + 2(Y_C - Y_C^2)/W_C}{0.5(Y_H^1 - Y_H^2)/W_H + 2(Y_C^1 - Y_C^2)/W_C} \quad (11)$$

where  $Y$  and  $W$  are mass fraction and molecular weight. Subscripts C and H refer to the carbon and hydrogen elements. Superscripts 1 and 2 refer the fuel and oxidizer, respectively. For making up the CD library, a series of stoichiometric ratio scalar dissipation rate are given for considering the effects of stretch on flames in the  $Z$  space. Then flamelets are obtained by transforming all the one-dimensional flame solutions into the  $Z - \mathcal{Y}$  space, where  $\mathcal{Y}$  is defined by the linear combination of steady state products of  $\text{CO}_2$  and  $\text{CO}$ .

$$\mathcal{Y} = \frac{Y_{\text{CO}_2}}{M_{\text{CO}_2}} + \frac{Y_{\text{CO}}}{M_{\text{CO}}} \quad (12)$$

To incorporate non-adiabatic effects, a third parameter  $\delta_h$  related to enthalpy loss is introduced. The enthalpy defect is defined by the difference between the enthalpy of the initial mixture for adiabatic and non-adiabatic conditions,<sup>37</sup>

$$\delta_h = h - [h_{\text{oxid}} + Z(h_{\text{fuel}} - h_{\text{oxid}})] \quad (13)$$

where  $h$ ,  $h_{\text{fuel}}$ , and  $h_{\text{oxid}}$  are enthalpy boundary, enthalpy of fuel and enthalpy of oxidizer, respectively. The latter two are defined in terms of absolute enthalpy. Enthalpy loss  $\delta_h$  take five points of 0, -5, -20, -50, -75  $\text{kJ kg}^{-1}$  for the consideration of the adiabatic to extreme non-adiabatic conditions.<sup>37</sup> To build a CD

library, the conditions imposed on the fuel side ( $Z = 1$ ) and the oxidation side ( $Z = 0$ ) are,

$$\begin{cases} Y_i = Y_i^{\text{fuel}}, h = h_{\text{fuel}} + \delta_h & \text{when } Z = 0 \\ Y_i = Y_i^{\text{oxid}}, h = h_{\text{oxid}} + \delta_h & \text{when } Z = 1 \end{cases} \quad (14)$$

The same strategy applies to the enthalpy conditions of the UP flame, but different mixture fractions imply a range of equivalence ratios, where fuel and oxidant get mixed side,

$$\begin{cases} Y_i = ZY_{\text{fuel}} + (1-Z)Y_{\text{oxid}} \\ h = Zh_{\text{fuel}} + (1-Z)h_{\text{oxid}} + \delta_h \end{cases} \quad (15)$$

Finally, the TCRI is accounted through the joint PDF of the independent variables. By applying  $\beta$ -PDF to mixture fraction and  $\delta$ -PDF to other control variables, the Favre-averaged/filtered scalars  $\phi$  is expressed as

$$\begin{aligned} \tilde{\phi} &= \int_{\delta_h \text{min}}^0 \int_0^1 \int_0^1 \phi(\delta_h, Z, C) \tilde{P}(\delta_h) \tilde{P}(Z) \tilde{P}(C) d\delta_h dZ dC \\ &= \int_{\delta_h \text{min}}^0 \int_0^1 \int_0^1 \phi(\delta_h, Z, C) \delta \left( \tilde{\delta}_h - \delta_h \right) \beta \left( Z, \tilde{Z}, \tilde{Z}'' \right) \\ &\quad \delta \left( \tilde{C} - C \right) d\delta_h dZ dC \end{aligned} \quad (16)$$

Where  $\mathcal{C}$  denotes normalized progress variable.

Based on the above methods, the pressure-based compressible solver is developed on the platform of OpenFOAM.<sup>38</sup> The pressure-velocity-density is solved through the PIMPLE algorithm.<sup>38</sup> The spatial accuracy is formally second-order.

## 2.3. Solution of $\text{NO}_x$

In the composition of  $\text{NO}_x$  emission, the amount of NO is one order of magnitude higher than that of the other components.<sup>16</sup> Therefore, the content of NO generally represents the  $\text{NO}_x$  emission. After trying various methods, an additional transport equation of NO mass fraction, as suggested by Ihme *et al.*<sup>24</sup> in their turbulent premixed flame simulation, gets solved in present work in order to improve the prediction accuracy.

$$\frac{\partial(\bar{\rho} \tilde{Y}_{\text{NO}})}{\partial t} + \frac{\partial(\bar{\rho} \tilde{u}_i \tilde{Y}_{\text{NO}})}{\partial x_i} = \frac{\partial}{\partial x_i} \left( D_{\text{NO}} \frac{\partial \tilde{Y}_{\text{NO}}}{\partial x_i} \right) + \bar{\rho} \tilde{\omega}_{\text{NO}} \quad (17)$$

where  $D_{\text{NO}}$  is effective dynamic viscosity of mixture. The chemical reaction source term of NO,  $\dot{\omega}_{\text{NO}}$ , is obtained by interpolation in flamelet library. See Section 3.1 for details on establishment of the  $\dot{\omega}_{\text{NO}}$  database. When the enthalpy loss is 0  $\text{kJ kg}^{-1}$ , the distribution of  $\dot{\omega}_{\text{NO}}$  in the  $Z - \mathcal{C}$  space is shown in Fig. 4. The detailed  $\text{CH}_4/\text{air}$  mechanism adopted in present work is GRI-2.11 (ref. 39) that shows more accurate results on  $\text{NO}_x$  emission<sup>40</sup> compared to GRI-3.0.<sup>41</sup>

## 2.4. Computational domain and numerical setup

Present investigation case is Sandia Flame D<sup>42</sup> and the burner schematic is shown in Fig. 1. The axisymmetric piloted burner has a main jet inner diameter ( $D$ ) of 7.2 mm. The pilot annulus

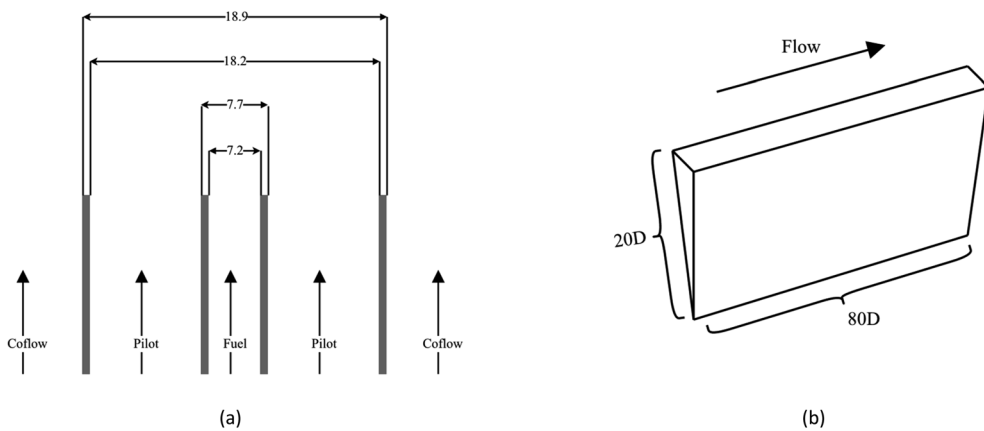


Fig. 1 The burner schematic in cross section view (a) and axis view (b) of the Sandia Flame D.

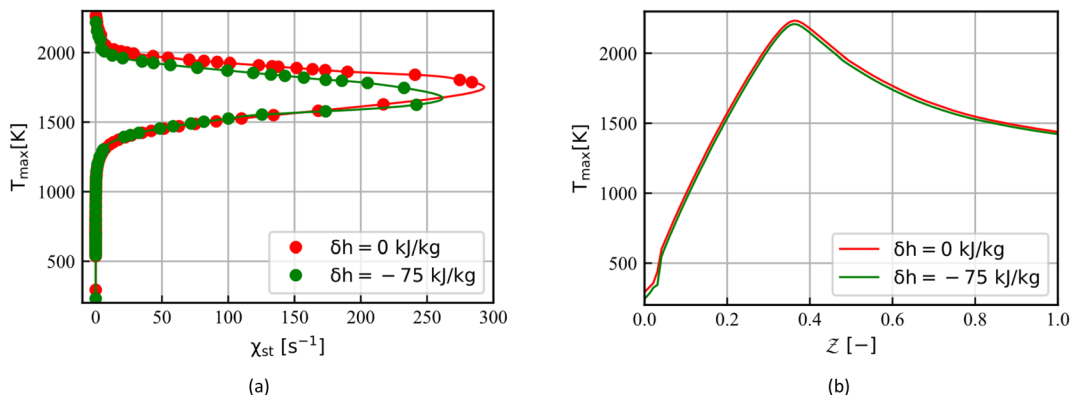


Fig. 2 The distributions of  $T_{\max}$  in CD flamelets (a) and in UP flamelets (b).

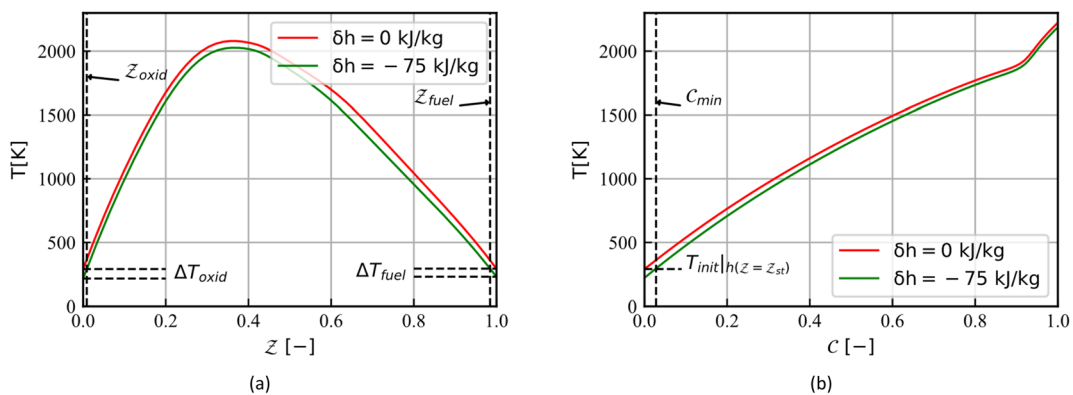


Fig. 3 Temperature profiles for CD flamelet with  $\chi_{\text{st}} = 4.5$  (a), and for UP flamelet with  $z = 0.35$  (b).

inner diameter and outer diameter is 7.7 mm and 18.2 mm, respectively. The burner outer wall diameter is 18.9 mm. Computational domain is a wedge with  $5^\circ$  and its axial and radial length is  $80D \times 20D$ . Grid cells around the axis and has a resolution of  $162 \times 1 \times 500$ . The mesh has a minimum grid of 0.125 mm and a total cell number of 81 000. Based on Reynolds numbers of 22 400, air-coflow, piloted jet and main fuel jet have bulk inflow velocity of  $0.9 \text{ m s}^{-1}$ ,  $11.4 \text{ m s}^{-1}$  and  $49.6 \text{ m s}^{-1}$ , and

have inflow temperature of 291 K, 1880 K and 294 K, respectively. The velocities of coflow and main fuel jet are under the standard state of 294 K, 0.993 atm. The pilot bulk velocity is estimated from the specified conditions, the flow area of the pilot annulus and the measured mass flow rates. The ambient pressure is 0.996 atm. Fuel is  $\text{CH}_4/\text{air}$  mixtures with a volume ratio of 1 : 3 ( $z = 1$ ). The piloted jet is burned mixtures containing  $\text{C}_2\text{H}_2$ ,  $\text{H}_2$ , air,  $\text{CO}_2$  and  $\text{N}_2$  ( $z = 0.271$ ). The pressure



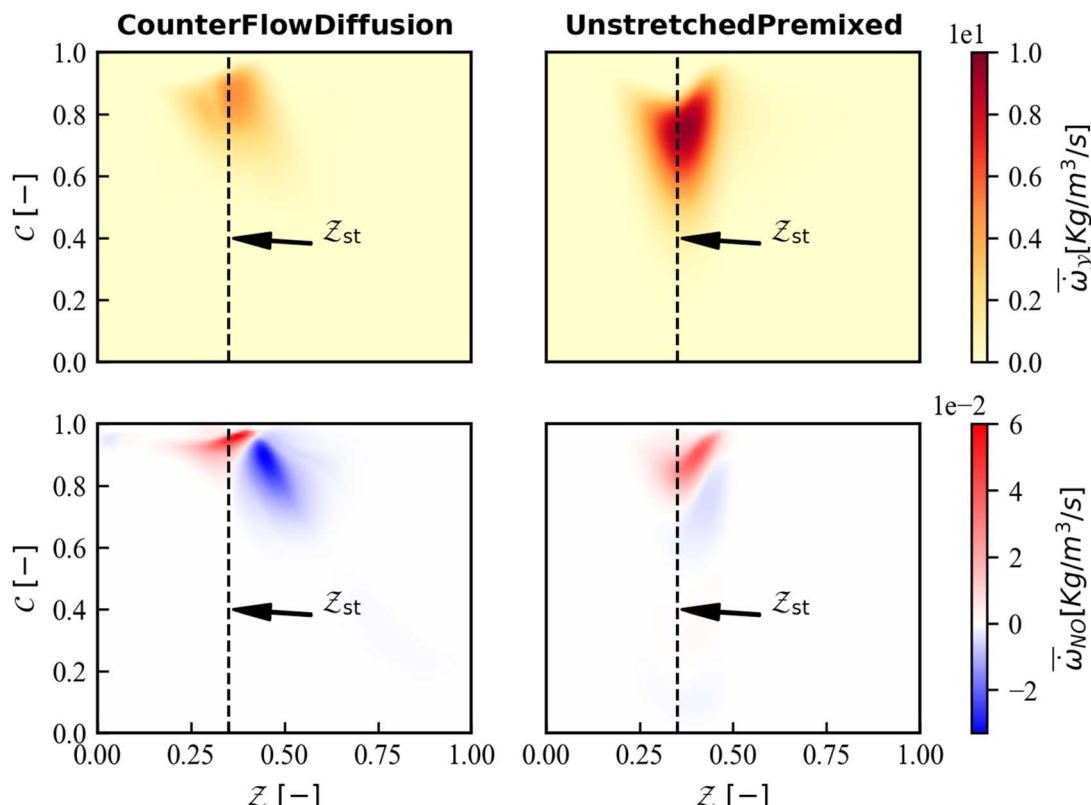


Fig. 4 Scatter point representation in  $Z - C$  space.

inlet boundary condition adopts the Neumann condition, and the pressure outlet boundary condition adopts the Dirichlet condition. The inlet boundary condition of other solution variables adopts Dirichlet condition, the outlet boundary condition adopts Neumann condition, and the wall adopts no-slip wall condition. Specifically, the  $k$  and  $\varepsilon$  use the wall function. Periodic boundary conditions are used on the left and right sides.

On the discretization of flamelet library, the mixture fraction and normalized progress variables have 101 uniform levels, and 11 points are used for the discretization of the variance of mixture fraction, which is further refined around the 0. Finally, the flamelet library resolution is set to  $\delta_h \times Z \times \zeta \times C = 5 \times 101 \times 11 \times 101$  points and a 4-order linear-interpolation is used when this library get coupled with the CFD solver.

### 3. Results and discussion

#### 3.1. Pre-processing for non-adiabatic flamelet library

Flamelet-like methods share a basic idea that the local turbulent flame can be identified as a set of one-dimensional flames. In other words, the multi-dimensional turbulent flame can be viewed as a series of one-dimensional laminar flames embedded in turbulent flow. Based on this assumption, two one-dimensional laminar flame are solved by FlameMaster<sup>34</sup> with the unity Lewis number assumption (equal diffusivities for

temperature and all species). The CD flame depends on the stoichiometric scalar dissipation rate  $\chi_{st}$ . Therefore, a series of CD flame are solved to generate the CD flamelet library. Fig. 2a shows the maximum temperature ( $T_{max}$ ) in the one-dimensional flame solution as a function of the  $\chi_{st}$ . Here, the upper half of the curve represents the steady-state flamelet solutions and the lower half of the curve represents the unsteady flamelet solutions. The stoichiometric scalar dissipation rate  $\chi_{st}$  in each flamelet calculation is given manually. The UP flame solution depends on the composition of the initial mixture, and then it is generated by solving the laminar steady UP flames under different ratios of fuel and oxidizer. Fig. 2b gives the  $T_{max}$  in the UP flame solution as a function of the mixture fraction. The thermochemical solutions beyond the flammability limit of laminar UP flames are obtained by extrapolation. These methods of generating flamelet library has received good feedback in many studies.<sup>37</sup>

In Section 2.3, we propose a method to reduce the absolute enthalpy of the boundary to get the non-adiabatic flamelet solutions. Since the predicted temperature is closely related to  $\text{NO}_x$  emissions, a maximum temperature analysis is performed firstly for two libraries. Fig. 2 shows the maximum temperature of each flamelet for a set of boundary conditions with enthalpy loss of 0  $\text{kJ kg}^{-1}$  and  $-75 \text{ kJ kg}^{-1}$ . As shown in Fig. 2a, the temperature loss of CD flamelets increases with the  $\chi_{st}$  growing up. However, a uniform drop of the maximum temperature in the UP flamelet solutions is observed in Fig. 2b. Based on the



definition of absolute enthalpy and the given boundary conditions, an enthalpy loss of  $-75 \text{ kJ kg}^{-1}$  is expected to reduce the temperature in Flame D simulation by about 50 K. This indicates that the CD flame solutions overestimate heat losses in the non-adiabatic flamelets generation.

As shown in Fig. 3, the inlet temperature of the laminar flame does not conform to the physical reality with the enthalpy loss treatment at the boundary. Fig. 3a shows the temperature of the CD flamelets as a function of the mixture fraction, the stoichiometric scalar dissipation rate is taken as 4.5. It can be seen that the temperature of the fuel side ( $\mathcal{Z} = 1$ ) and the oxidant side ( $\mathcal{Z} = 0$ ) has a local temperature drop with the enthalpy loss  $-75 \text{ kJ kg}^{-1}$ , the fuel side is lower than 294 K and the oxidant side is lower than 291 K. In Fig. 3b, the initial mixture of the UP flame is taken as the mixture fraction 0.35 and the temperature as a function of the normalized reaction progress variable. Similarly, the temperature at the initial side ( $\mathcal{C} = 0$ ) is lower than 291 K with the enthalpy loss  $-75 \text{ kJ kg}^{-1}$ . Many thermochemical parameters are temperature dependent, such as species mass fractions, chemical reaction source term, and especially for  $\text{NO}_x$  emission. Thus, this part of the solution that does not conform to physical reality requires special treatment. In the following, two steps are taken to generate the corrected non-adiabatic CD flamelet profile:<sup>37</sup>

- (i) Delete the parts of solution that has non-physical temperature;
- (ii) Correct the mixture fraction range from [0–1] to  $[\mathcal{Z}_{\text{oxid}} - \mathcal{Z}_{\text{fuel}}]$  for presumed PDF integration.

Similarly, correct the normalized process variables range from [0–1] to  $[\mathcal{C}_{\min} - 1]$  for non-adiabatic UP library. This treatment has a very negligible effect on simulation results.<sup>37</sup>

Two libraries applied in simulations are obtained with above mentioned special processing method. As shown in Fig. 4, the reaction progress variable source and the NO source that are used for CFD calculation are compared in the  $\mathcal{Z} - \mathcal{C}$  space, where the enthalpy loss is  $0 \text{ kJ kg}^{-1}$ . Compared with the UP flame, the NO sources in the CD library are more widely distributed and closer to the steady state reaction region ( $\mathcal{C} = 1$ ). The explanation for this is that the CD flame with stretching effect underestimates the progress variable source and overestimates the NO source.

### 3.2. Effects of flamelet library on flame structure

In this section, the mean temperature and mean mass fraction of  $\text{CO}_2$ ,  $\text{H}_2\text{O}$  and  $\text{NO}$  measured at the axis and at various axial positions are compared with the steady state numerical results to evaluate the effect of different laminar flamelet libraries on combustion simulations. The screenshots of steady temperature and the mass fraction of  $\text{NO}$  at the mid-plane of the domain give clear flame structure. Unlike the mass fraction of  $\text{NO}$  that is updated by an additional transport equation, steady state products such as  $\text{CO}_2$  and  $\text{H}_2\text{O}$  are look-up directly from the libraries.

**3.2.1. Flame structure.** Fig. 5a shows the numerical mean temperature distribution of the flow at the mid-plane of the domain. The upper half simulation results is obtained from the UP library and the lower half is obtained from the CD library. The comparison shows that the mean temperature distributions in upstream ( $z/D < 30$ ) obtained by two libraries are very close. The temperatures are over-predicted by CD library from the end of injection jet ( $z/D > 30$ ), which is about 100 K higher than the UP library. Fig. 5b shows the temperature profiles on the central axis. The temperature predicted by the UP library shows good agreement with the upstream and downstream experimental data, except for a slight overestimation around  $z/D = 30$ . Further efforts can be made to improve the simulated flow field. However, present study mainly discusses the dependence of  $\text{NO}$  simulation results on the flamelet library. Therefore, on the premise that the global temperature predicted by the UP library is acceptable, we pay more attention to the deviation of the temperature field predictions of the CD and UP library. Obviously, there is a generally over-prediction in the numerical solution for the CD library ( $20 < z/D < 40$ ).

The radial mean temperature plots at the  $z/D$  locations of 3, 15, 30, 45, 60 and 75 are shown in Fig. 6. These locations include the entire flow field, especially the last four points are where the main flame structure exists, which can better indicate the performance of the combustion model. Simulation results are compared with experimental data. At the location of  $z/D = 3$ , both the flamelet libraries predict well. They also give temperature distributions in agreement with experimental values at the locations of  $z/D = 15$  and  $z/D = 45$ . However, the simulation temperature is higher than the experimental data at the locations of  $z/D = 30$  for  $0 \leq r/D \leq 2$ , especially the overestimation of

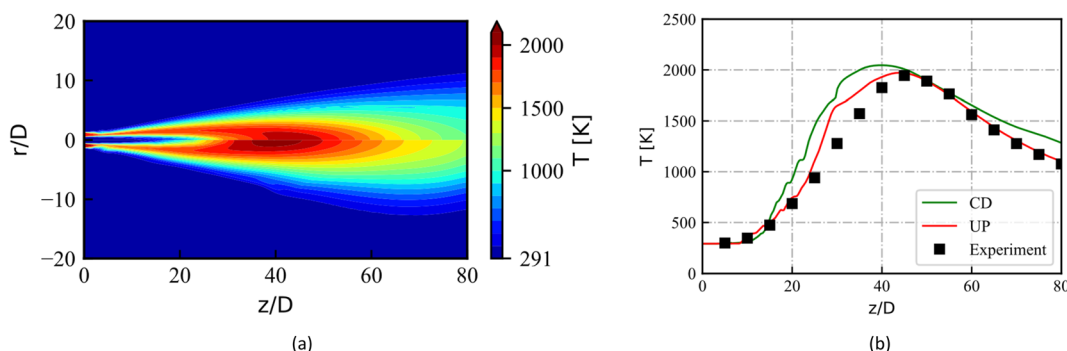


Fig. 5 (a) The temperature distribution obtained from numerical simulation based on the two libraries. The upper part is from UP library and the lower part is from CD library. (b) The temperature profiles on the central axis. Red line marks UP library, green line marks CD library.



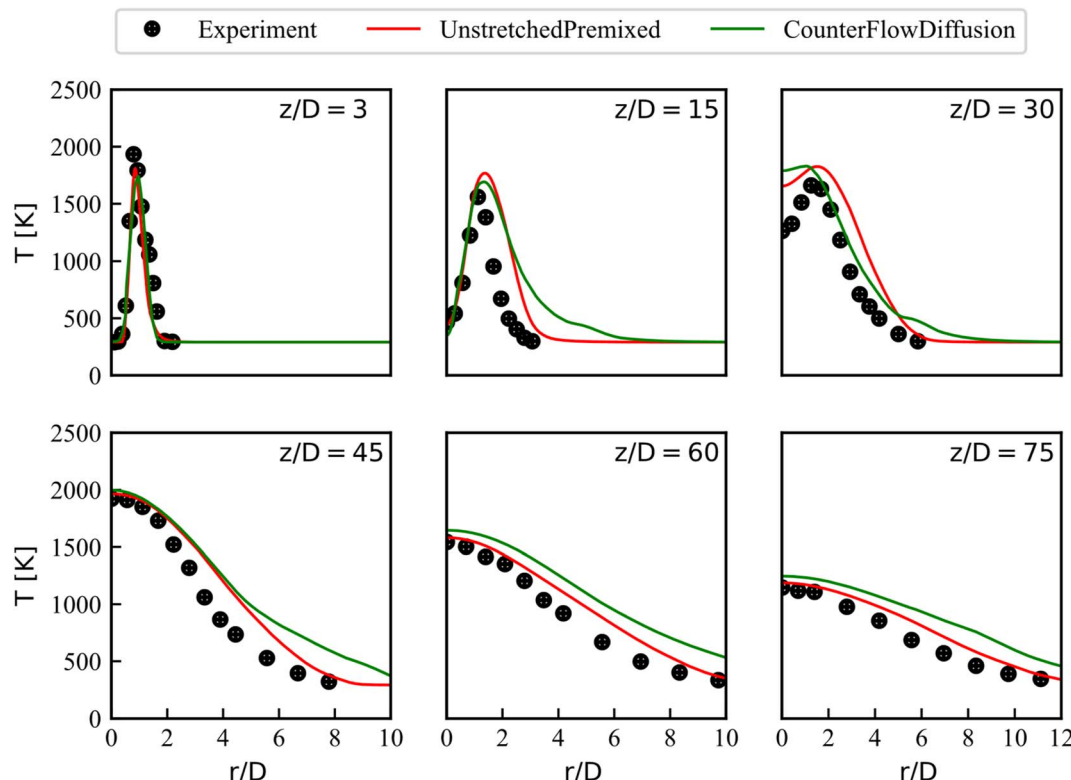


Fig. 6 Radial profiles of temperature at six different locations along the axis.

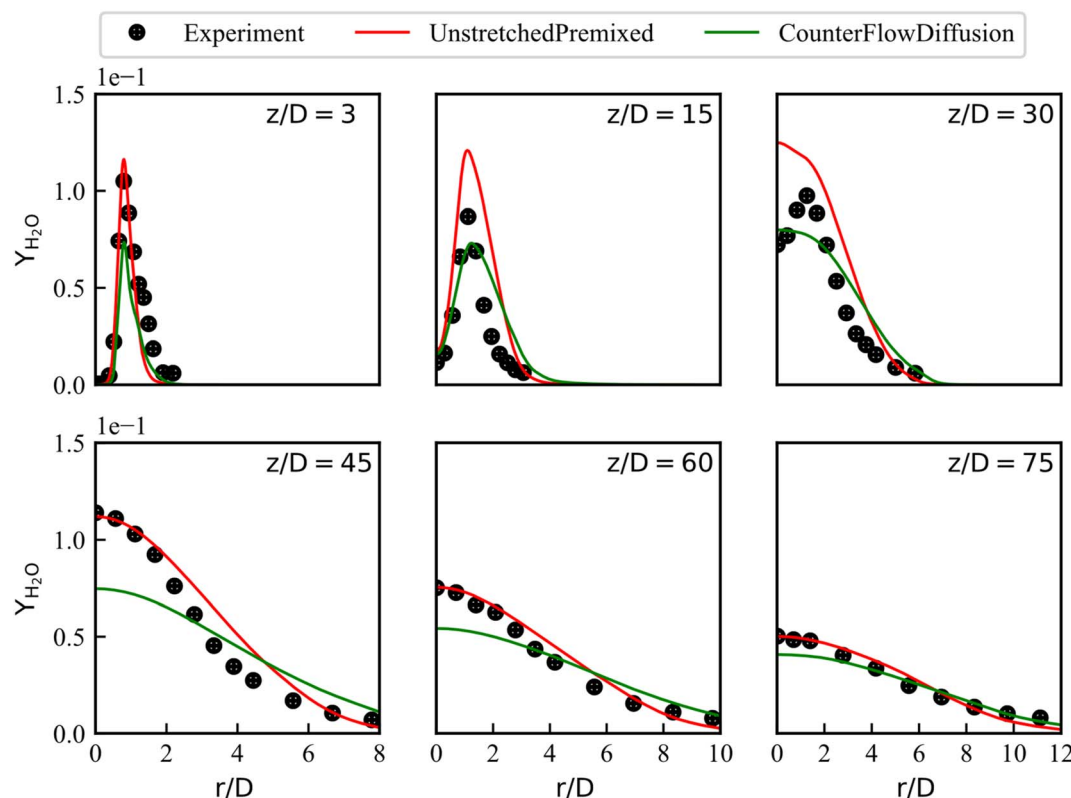


Fig. 7 Radial profiles of mass fraction of  $\text{H}_2\text{O}$  at six different locations along the axis.



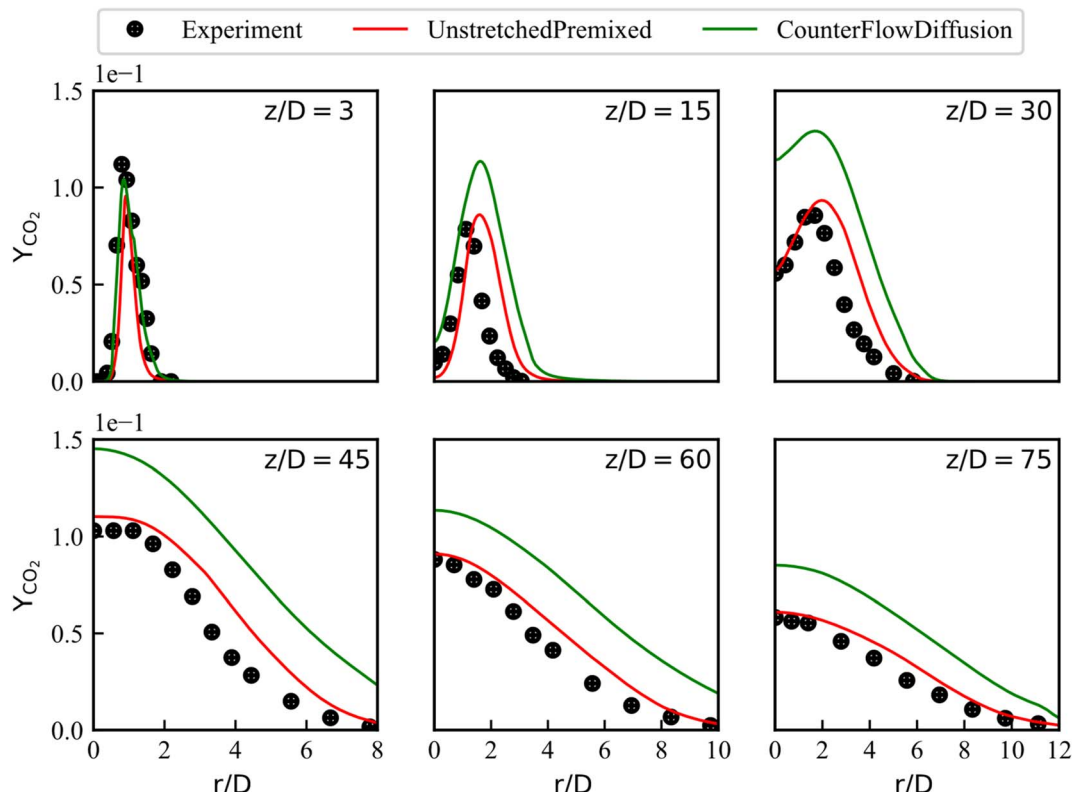


Fig. 8 Radial profiles of mass fraction of  $\text{CO}_2$  at six different locations along the axis.

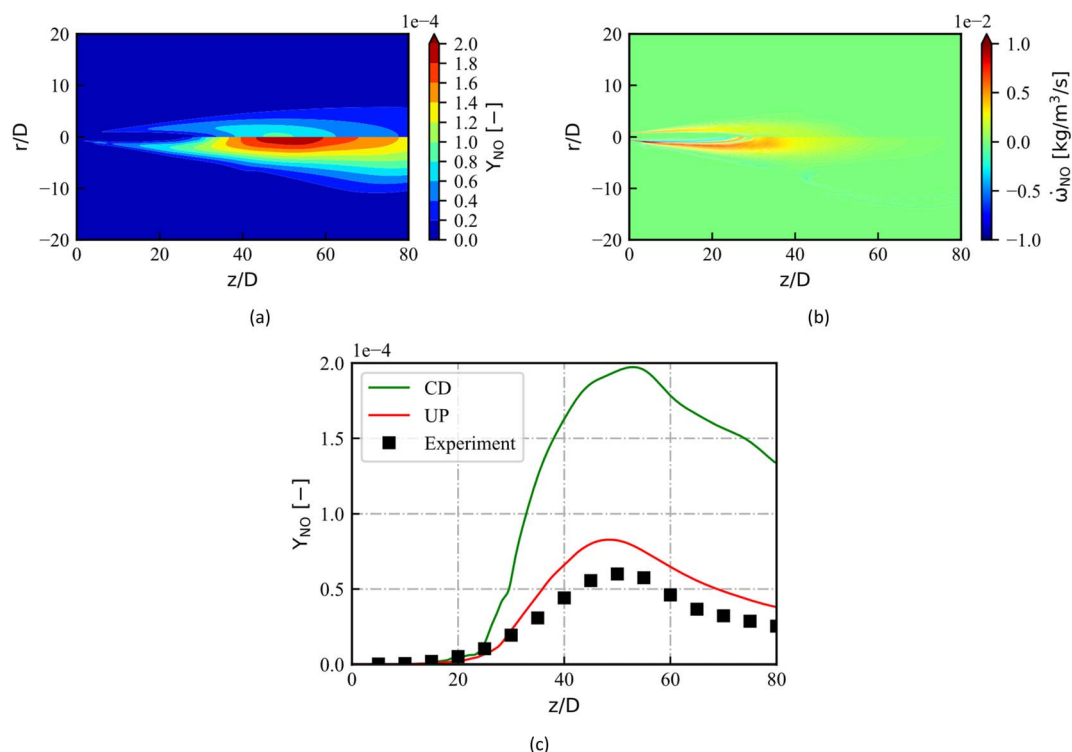


Fig. 9 (a) The distribution of the mass fraction of NO, the upper part is from UP library and the lower part is from CD library. (b) The distributions of the NO source. (c) The NO profiles on the central axis, red line marks UP library, green line marks CD library.

the CD library is more serious. Errors can be reduced by choosing other turbulence and combustion models, but this is beyond the purpose of the present work. At positions of  $z/D = 60$  and  $z/D = 75$ , the CD-based simulation results are higher than the UP-based results in the entire radial direction. Overall, these radial data support the conclusion that the UP library predict better temperature profiles.

The radial mean mass fractions of  $\text{CO}_2$ ,  $\text{H}_2\text{O}$  are compared with the experiments in Fig. 7 and 8, respectively. The numerical results of steady state products obtained from the UP library matched the experimental values well at all locations except at location of  $z/D = 30$ , where the mass fraction of  $\text{H}_2\text{O}$  is overestimated, especially around  $r/D = 2$ . The larger errors in radial profiles of temperature and  $\text{H}_2\text{O}$  are mainly manifested at location of  $z/D = 30$  close to the central axis. The reasons for these errors are different. The overestimated temperature can be explained that the turbulence model underestimates the penetration distance of the scalar field, causing the high temperature zone to be closer to the upstream. But the global temperature profile trend is consistent with the experimental data. However, for the  $\text{H}_2\text{O}$  profile at the same location in Fig. 7, the trend is inconsistent with the experimental data.

Fig. 7 shows that it is difficult to capture the peak of  $\text{H}_2\text{O}$  concentration distribution near the central axis at  $z/D = 30$ . This phenomenon should be analyzed together with Fig. 8 (the distribution of  $\text{CO}_2$  concentration) and the definition of progress variable (eqn (12)) that includes  $\text{CO}_2$  and not includes  $\text{H}_2\text{O}$ . Therefore, the progress variable field obtained by the transport

equation can well reproduce the distribution of  $\text{CO}_2$ , such as the good agreement between UP predicted  $\text{CO}_2$  and experimental data, as shown in Fig. 8. In contrast, the mass fractions of species interpolated by the library, such as  $\text{H}_2\text{O}$ , cannot reproduce the experimental peaks in some local flow fields, which is the reason for the additional transport equation of NO mass fraction.

With the CD library, the simulation results underestimate the mass fraction of  $\text{H}_2\text{O}$  at the peak, while systematically overestimating the mass fraction of  $\text{CO}_2$  in the radical direction. In general, URANS coupled with the UP library are feasible method for pilot jet combustion modeling.

**3.2.2.  $\text{NO}_x$  emission.** An additional transport equation is expected to accurately predict the mass fraction of NO,  $Y_{\text{NO}}$ , as discussed in Section 2.3. Fig. 9a and b gives visualization of the  $\text{NO}_x$  distribution with snapshot of  $Y_{\text{NO}}$  and the NO source ( $\dot{\omega}_{\text{NO}}$ ), respectively. The mean  $Y_{\text{NO}}$  obtained from the two libraries are very close in the upstream of the fuel jet ( $z/D < 15$ ). The distribution of  $\dot{\omega}_{\text{NO}}$  shows a large difference in shear layer, where represent regions of high scalar dissipation rates. The noticeable difference starts at the end of jet ( $z/D > 30$ ), where the maximum value of  $Y_{\text{NO}}$  in the CD library is overestimated and has a wider distribution. Notably, the maximum value of  $\dot{\omega}_{\text{NO}}$  in the CD library (Fig. 9b) is only 10% larger than that in the UP library, but four times larger in  $Y_{\text{NO}}$  (Fig. 9a). The distributions of  $Y_{\text{NO}}$  on the central axis are shown in Fig. 9c. The two distributions of  $Y_{\text{NO}}$  on the centerline are close to each other at the beginning of the jet ( $z/D < 25$ ). However, the prediction of  $Y_{\text{NO}}$  of

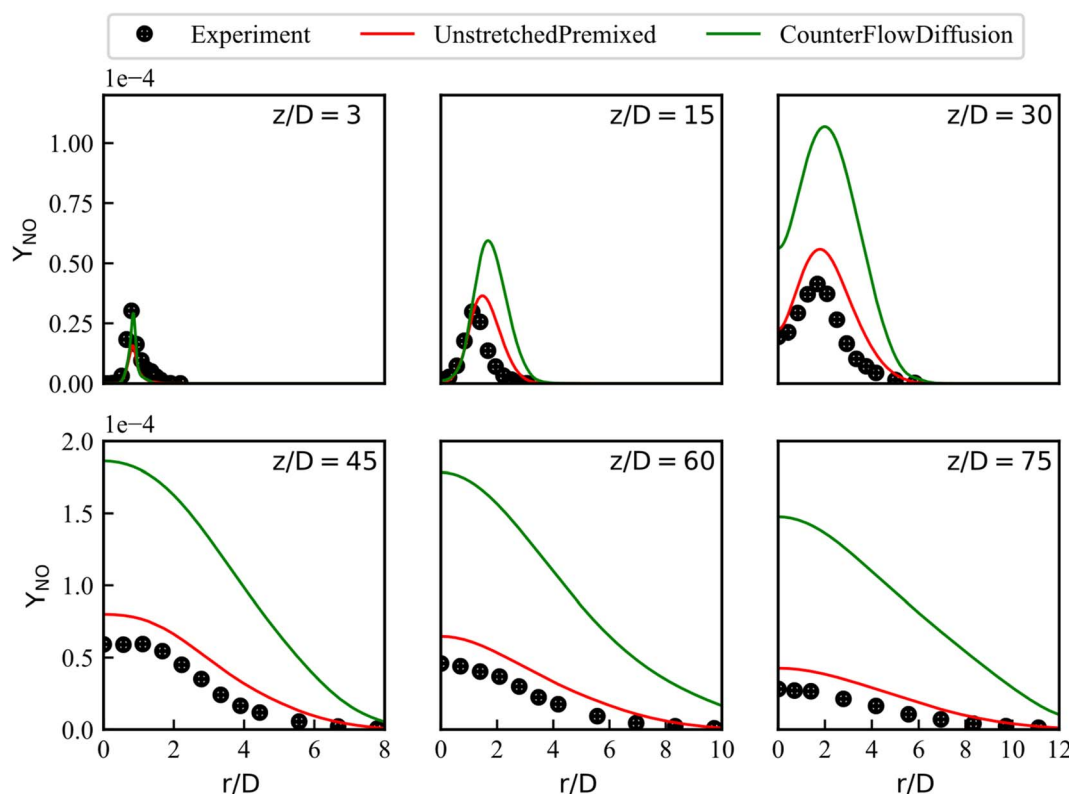


Fig. 10 Radial profiles of mass fraction of NO at six different locations along the axis.



the UP library are much better where  $NO_x$  emissions start to rise ( $z/D > 30$ ).

The experimental data of  $Y_{NO}$  are available at the axial locations of  $z/D = 3, 15, 30, 45, 60$  and  $75$ , they are compared with the numerical profiles of  $Y_{NO}$  in Fig. 10. The simulated  $Y_{NO}$  with the CD library significantly overestimated NO emissions at locations of  $z/D \geq 30$ . Overall, the contours and centerline sampling of the mean  $Y_{NO}$  with UP library are consistent with experimental results. Compared with the 4.2 times overestimation of the maximum error in CD prediction of NO mass fraction, the UP prediction accuracy improved to 0.5 times overestimation referring to the experimental data. Details are shown in Table S1 and Fig. S2<sup>†</sup> in the ESI.<sup>†</sup>

The differences in  $Y_{NO}$  predictions are mainly attributed to the differences in  $\dot{\omega}_{NO}$  predictions. The RANS simulation results coupled CD library overestimate the temperature when  $z/D = 20\text{--}40$ . Considering the thermal NO mechanism, high temperature causes the NO source term increase, as shown in Fig. 5 and 9. Moreover, the actual combustion of the Sandia Flame D is complicated. As a pilot flame, there are both diffusion combustion and partial premixed combustion, as well as premixed combustion mode. In the high temperature region of Flame D, the actual  $NO_x$  chemistry mainly dominated by the premixed combustion mode, so UP library gives a better estimation of  $NO_x$ .

Analysis of the distribution of  $Y_{NO}$  shows that the library that is generated by the method of converting laminar CD flamelets with different stoichiometric scalar dissipation rates into  $\mathcal{J} - \mathcal{Y}$  space has drawback on the prediction of  $NO_x$  emissions. The UP library is a better modeling choice for accurate prediction of slow reaction product which are dominated by chemistry.

## 4. Conclusions

The numerical investigation of a turbulent pilot jet flame (Sandia Flame D) is carried out by developing a custom URANS solver in present study. The turbulence model adopts the standard  $k\text{--}\varepsilon$  model, and the combustion model adopts the flamelet chemistry tabulation method to avoid expensive chemical reaction integration costs. The absolute enthalpy and the mass fraction of species are obtained by interpolation from the library. To improve the prediction accuracy, the mass fraction of NO is solved by an additional transport equation. Two 4D non-adiabatic flamelet libraries are generated from the 1D laminar UP flame and the 1D laminar CD flame, respectively. Compared with the experimental data, the influence of the flamelet databases generated by different types of flamelets on the simulation results are discussed.

The simulation results show that the NO field depends on the laminar flamelet type. Two 4D flame libraries provided almost the same range of values in terms of temperature and major species fields. The NO source term  $\dot{\omega}_{NO}$  in UP library introduces a reasonable agreement with measurement data by solving an additional NO transport equation. However, the 1D laminar CD flamelet solutions with detailed chemical mechanism introduces a larger value of  $\dot{\omega}_{NO}$  and over-predicted  $Y_{NO}$  in simulations. Overall, URANS simulations based on the non-

adiabatic 4D library of UP flamelet and the standard  $k\text{--}\varepsilon$  turbulence model can provide a high-precision prediction of  $NO_x$  emission. The current study clearly demonstrates the feasibility of predicting  $NO_x$  emissions using tabulated chemistry methods, and the unpredictable  $NO_x$  emissions are numerically reproduced through a non-adiabatic library based on UP flames. The proposed method can be applied to high-precision numerical simulation of  $NO_x$  emission for other engineering combustors.

## Conflicts of interest

There are no conflicts to declare.

## Acknowledgements

This work is supported by the National Natural Science Foundation of China (No. 91741201).

## References

- 1 S. Iavarone and A. Parente, *Front. Mech. Eng.*, 2020, **6**, 13.
- 2 M. Ravikanti, M. Hossain and W. Malalasekera, *Proc. Inst. Mech. Eng., Part A*, 2009, **223**, 41–54.
- 3 T. Lu and C. K. Law, *Prog. Energy Combust. Sci.*, 2009, **35**, 192–215.
- 4 H. Xue and S. K. Aggarwal, *Combust. Flame*, 2003, **132**, 723–741.
- 5 H. Guo and G. J. Smallwood, *Int. J. Therm. Sci.*, 2007, **46**, 936–943.
- 6 V. Fichet, M. Kanniche, P. Plion and O. Gicquel, *Fuel*, 2010, **89**, 2202–2210.
- 7 M. Zhang, Z. Fu, Y. Lin and J. Li, *Chin. J. Aeronaut.*, 2012, **25**, 854–863.
- 8 Y. Kang, Q. Wang, X. Lu, H. Wan, X. Ji, H. Wang, Q. Guo, J. Yan and J. Zhou, *Appl. Energy*, 2015, **149**, 204–224.
- 9 A. Innocenti, A. Andreini, D. Bertini, B. Facchini and M. Motta, *Fuel*, 2018, **215**, 853–864.
- 10 S. Iavarone, M. Cafiero, M. Ferrarotti, F. Contino and A. Parente, *Int. J. Hydrogen Energy*, 2019, **44**, 23436–23457.
- 11 E. C. Okafor, K. D. K. A. Somaratne, R. Ratthanan, A. Hayakawa, T. Kudo, O. Kurata, N. Iki, T. Tsujimura, H. Furutani and H. Kobayashi, *Combust. Flame*, 2020, **211**, 406–416.
- 12 C. Schluckner, C. Gaber, M. Landfahrer, M. Demuth and C. Hochauer, *Fuel*, 2020, **264**, 116841.
- 13 A. B. Wakale, S. Banerjee and R. Banerjee, *J. Energy Inst.*, 2020, **93**, 1868–1882.
- 14 M. Sripathi, S. Krishnaswami, A. M. Danis and S.-Y. Hsieh, in *Turbo Expo: Power for Land, Sea, and Air*, American Society of Mechanical Engineers, 2014, vol. 45691, p. V04BT04A060.
- 15 R. Saini, S. Prakash, A. De and R. Yadav, *Therm. Sci. Eng. Prog.*, 2018, **5**, 144–157.
- 16 A. C. Zambon, B. Muralidharan, A. Hosangadi and K. Ajmani, in *AIAA Propulsion and Energy 2020 Forum*, American Institute of Aeronautics and Astronautics, 2020.



- 17 O. Gicquel, N. Darabiha and D. Thévenin, *Proc. Combust. Inst.*, 2000, **28**, 1901–1908.
- 18 N. Peters, *Prog. Energy Combust. Sci.*, 1984, **10**, 319–339.
- 19 C. D. Pierce and P. Moin, *J. Fluid Mech.*, 2004, **504**, 73–97.
- 20 J. A. van Oijen, A. Donini, R. J. M. Bastiaans, J. H. M. ten Thije Boonkamp and L. P. H. de Goey, *Prog. Energy Combust. Sci.*, 2016, **57**, 30–74.
- 21 J. A. V. Oijen and L. P. H. D. Goey, *Combust. Sci. Technol.*, 2000, **161**, 113–137.
- 22 G. Godel, P. Domingo and L. Vervisch, *Proc. Combust. Inst.*, 2009, **32**, 1555–1561.
- 23 v. J. A. Oijen and d. L. P. H. Goey, *Proceedings of the European Combustion Meeting*, 2009.
- 24 M. Ihme and H. Pitsch, *Phys. Fluids*, 2008, **20**, 055110.
- 25 H. Yigit Akargun, B. Akkurt, N. G. Deen and L. M. T. Somers, in *The Proceedings of the International symposium on diagnostics and modeling of combustion in internal combustion engines*, The Japan Society of Mechanical Engineers, 2017, p. A105.
- 26 J. Tang and W. Song, *J. Propul. Technol.*, 2017, **38**, 1523–1531.
- 27 Q. Yao, Y. Zhang, X. Wang, Z. Tian, G. Hu and W. Du, *Neurocomputing*, 2022, **482**, 224–235.
- 28 Z. An, M. Zhang, W. Zhang, R. Mao, X. Wei, J. Wang, Z. Huang and H. Tan, *Fuel*, 2021, **304**, 121370.
- 29 W. Zhang, S. Karaca, J. Wang, Z. Huang and J. van Oijen, *Combust. Flame*, 2021, **227**, 106–119.
- 30 H. Jasak, *PhD thesis*, Imperial College London (University of London), 1996.
- 31 H. G. Weller, G. Tabor, H. Jasak and C. Fureby, *Comput. Phys.*, 1998, **12**, 620.
- 32 W. P. Jones and B. E. Launder, *Int. J. Heat Mass Transfer*, 1972, **15**, 301–314.
- 33 W. L. Grosshandler, *RADCAL: A Narrow-Band Model for Radiation Calculations in a Combustion Environment*, 1993.
- 34 P. J. Coelho, O. J. Teerling and D. Roekaerts, *Combust. Flame*, 2003, **133**, 75–91.
- 35 H. Pitsch, *FlameMaster, A C++ Computer Program for 0D Combustion and 1D Laminar Flame Calculations*.
- 36 R. W. Bilger, *Combust. Sci. Technol.*, 1976, **13**, 155–170.
- 37 S. K. Sadasivuni, *LES Modelling of Non-premixed and Partially Premixed Turbulent Flames*, Loughborough University, 2009.
- 38 T. Li, F. Kong, B. Xu and X. Wang, *Appl. Math. Mech.*, 2019, **40**, 1197–1210.
- 39 C. T. Bowman, R. K. Hanson, D. F. Davidson, W. C. Gardiner Jr, V. Lissianski, G. P. Smith, D. M. Golden, M. Frenklach and M. Goldenberg, *GRI-Mech 2.11*, [http://www.me.berkeley.edu/gri\\_mech/](http://www.me.berkeley.edu/gri_mech/).
- 40 R. V. Murthy, *Advanced Flamelet Modelling of Turbulent Nonpremixed and Partially Premixed Combustion*, Loughborough University, 2008.
- 41 G. P. Smith, D. M. Golden, M. Frenklach, N. W. Moriarty, B. Eiteneer, M. Goldenberg, C. T. Bowman, R. K. Hanson, S. Song, W. C. Gardiner Jr, V. V. Lissianski and Z. Qin, *GRI-Mech 3.0*, [http://www.me.berkeley.edu/gri\\_mech/](http://www.me.berkeley.edu/gri_mech/).
- 42 R. Barlow, J. Frank, A. Karpetis and J. Chen, *Combust. Flame*, 2005, **143**, 433–449.

